

Electrochemical Performance of $\text{Li}_{0.995}\text{Al}_{0.005}\text{Mn}_{0.85}\text{Fe}_{0.15}\text{PO}_4/\text{C}$ as a Cathode Material for Lithium-Ion Batteries

Yun-Fei Long^{1, 2}, Qiao-Ying Huang¹, Zhi Wu¹, Jing Su^{1, 2}, Xiao-Yan Lv³, Yan-Xuan Wen^{1, 2, *}

¹ School of Chemistry and Chemical Engineering, Guangxi University, Nanning 530004, PR China

² Guangxi Colleges and Universities Key Laboratory of Novel Energy Materials and Related Technology, Nanning 530004, PR China

³ The New Rural Development Research Institute, Guangxi University, Nanning 530004, PR China

* E-mail: wenyanxuan@vip.163.com

Received: 28 August 2016 / Accepted: 1 October 2016 / Published: 10 November 2016

A solid-state reaction route was used to prepare $\text{Li}_{0.995}\text{Al}_{0.005}\text{Mn}_{0.85}\text{Fe}_{0.15}\text{PO}_4/\text{C}$, and the prepared sample were characterized by X-ray diffraction (XRD), X-ray photoelectron spectroscopy (XPS), scanning electron microscopy (SEM) and electrochemical tests. The results of XRD and XPS show that Al^{3+} and Fe^{2+} are soluble in the Li site and the Mn site to generate a solid-solution, resulting in a shrinkage of crystal lattice and creations of Al^{3+} -vacancy pairs and Fe^{3+} -vacancy pairs. Compared with $\text{Li}_{0.995}\text{Al}_{0.005}\text{MnPO}_4/\text{C}$, $\text{LiMn}_{0.85}\text{Fe}_{0.15}\text{PO}_4/\text{C}$ and LiMnPO_4/C , $\text{Li}_{0.995}\text{Al}_{0.005}\text{Mn}_{0.85}\text{Fe}_{0.15}\text{PO}_4/\text{C}$ exhibits much better rate capability and cycling stability. When charged and discharged at 1 C, $\text{Li}_{0.995}\text{Al}_{0.005}\text{Mn}_{0.85}\text{Fe}_{0.15}\text{PO}_4/\text{C}$ delivers a discharge capacity of 139 and 160 $\text{mAh}\cdot\text{g}^{-1}$ at 25 and 60 °C, and its capacity retention ratio is 100 % after 50 cycles, respectively. The enhanced property of LiMnPO_4/C can be attributed to the synergistic effect of Al^{3+} doping at the Li site and Fe^{2+} doping at the Mn site, leading to a great improvement in the dynamic stability of the olivine structure, Li^+ diffusion and electrode kinetics. Thus, the electrochemical properties of lithium manganese phosphate can be effectively improved by Fe^{2+} doping at the Mn site and aliovalent ion doping at the Li site.

Keywords: Lithium ion batteries; Cathode; Lithium manganese phosphate; Cation substitution

1. INTRODUCTION

LiMnPO_4 has been researched as a potential cathode material for next-generation of Li-ion batteries due to its optimal redox potential (4.1 V vs. Li^+/Li), its energy density, which is approximately 20% larger than that of LiFePO_4 and its compatibility with most of the liquid electrolytes presently used in Li ion batteries [1, 2, 50]. However, LiMnPO_4 has poor rate capability owing to its low intrinsic electronic and ionic conductivity [2]. To improve the rate performance of

LiMnPO₄, following methods have been proposed [2-5]: (1) surface coating carbon layer; (2) reducing particle size and controlling the particle morphology; and (3) doping with guest ions. Among these adopted methods, doping with guest ion on Mn-site is an effective way to improve the electrochemical performance of LiMnPO₄ [6], and various metal ions such as Fe²⁺ [7-15], Mg²⁺ [12, 13, 15-24], Co²⁺ [12, 15, 25], Zn²⁺ [26, 27], Cu²⁺ [28, 29], Ce³⁺ [30], Cr³⁺ [31, 32], V³⁺ [15, 33-37], Ti⁴⁺ [24] and Zr⁴⁺ [23, 24, 38] have been applied to improve the electrochemical behavior of LiMnPO₄ [50]. Moreover, the performance of LiMnPO₄ can be effectively enhanced by co-doping on Mn-site, such as Fe²⁺-Mg²⁺ [38-46], Fe²⁺-Co²⁺ [47-48], Co²⁺-Mg²⁺ [49], Fe²⁺-Zn²⁺ [26], Fe²⁺-Ti⁴⁺ [50], Mg²⁺-Zr⁴⁺ [23]. For instance, the discharge capacity of LiMn_{0.9}Fe_{0.05}Mg_{0.05}PO₄ at 0.2 C was 121 mAh·g⁻¹, while that of LiMnPO₄ and LiMn_{0.9}Fe_{0.1}PO₄ was only 67 and 74 mAh·g⁻¹, respectively [46]. Huang et al. reported that Li(Mn_{0.85}Fe_{0.15})_{0.92}Ti_{0.08}PO₄/C delivered a capacity of about 144 mAh·g⁻¹ at 1 C, while LiMn_{0.85}Fe_{0.15}PO₄/C and LiMn_{0.92}Ti_{0.08}PO₄/C only delivered a capacity of 126 and 106 mAh·g⁻¹, respectively [50]. Clearly, the property of LiMnPO₄ can be enhanced by the synergistic effect between ions co-doping at the Mn-site, but the roles of multiple cations need to be further confirmed.

Several researchers reported that substitution of Li⁺ by Al³⁺ can effectively improve electrochemical performance of LiFePO₄ [51-55]. With the similarity of LiMPO₄ (M=Fe, Mn) and the previous works of co-doped LiMnPO₄ [23, 26, 38-50], we infer that a synergistic effect may exist between Fe doping at Mn site and Al doping at Li site, and the electrochemical performance of LiMnPO₄ may be further improved by Fe doping at Mn site and Al doping at Li site. Therefore, we synthesize and characterize Li_{0.995}Al_{0.005}Mn_{0.85}Fe_{0.15}PO₄/C that is in comparison with the LiMnPO₄/C, Li_{0.995}Al_{0.005}MnPO₄/C and LiMn_{0.85}Fe_{0.15}PO₄/C. The results in the present work demonstrate that the electrochemical performance of LiMnPO₄ can be significantly enhanced by the synergistic effect between Fe²⁺ doping at Mn site and Al³⁺ doping at Li site.

2. EXPERIMENTAL

A solid-state reaction method was applied to prepare Li_{1-x}Al_xMn_{1-y}Fe_yPO₄/C (x=0.000, 0.005; y=0.00, 0.15) composites. 19 wt% sucrose (AR, Beijing Chemical Reagent Co. LTD) was milled with a stoichiometric proportion of Li₂CO₃, MnC₂O₄·2H₂O, FeC₂O₄·2H₂O, Al₂O₃, NH₄H₂PO₄ in water by a stirred media mill for 3.5 h. The milled slurry was dried in a spray-drying unit. The dried mixture was sintered at 300 °C for 2 h, and then at 600 °C for 10 h under N₂ (99.999% purity).

Phase composition and crystal structure of the prepared samples were identified by a Rigaku D/Max 2500V diffractometer with Cu Kα (λ = 0.15406 nm) at 40 kV and 40mA. A scanning electron microscopy (SEM, S-3400N) was applied to observe the morphologies of the prepared samples. A EuroVector Euro EA 3000 elemental analyzer was used to measure the carbon content of the prepared samples. X-ray photoelectron spectra (XPS) of the prepared Li_{1-x}Al_xMn_{1-y}Fe_yPO₄/C were measured using a Thermo ESCALAB 250XI (Thermo fisher, USA). XPS spectra were analyzed with XPS Peak-fit software.

The cathode slurry was prepared by first mixing Li_{1-x}Al_xMn_{1-y}Fe_yPO₄/C, acetylene black and PVDF binder with the mass ratio of 80:10:10 in N-methyl-2-pyrrolidone (NMP, Aldrich). The slurry

was cast onto an aluminum current collector and then dried at 120 °C for 12 h under vacuum. The charge/discharge behaviors of the prepared samples were tested using CR2032 coin cells containing a cathode, a Celgard 2300 membrane as the separator, a lithium foil anode, and the electrolyte (1 mol L⁻¹ LiPF₆ in EC/DMC (1:1 by volume)). The cyclic voltammetry (CV) and electrochemical impedance spectroscopy (EIS) experiments were performed using the three electrode cell (ECC-REF, EL-Cell GmbH, Germany). The details of the synthesis process, materials characterization and the electrochemical experiments were described by Huang et al [50].

3. RESULTS AND DISCUSSION

3.1. Structure and morphology

LiMnPO₄/C, LiMn_{0.85}Fe_{0.15}PO₄/C, Li_{0.995}Al_{0.005}MnPO₄/C and Li_{0.995}Al_{0.005}Mn_{0.85}Fe_{0.15}PO₄/C were prepared to study the effects of Fe and/or Al doping on the structure and performance, and the corresponding samples was named as LMP, LMFP, LAMP and LAMFP, respectively. XRD was used to investigate the effects of Fe and/or Al doping on the phase, and the instrument error during the XRD experiments was corrected by the standard silicon powder [50]. The XRD patterns of LMP, LMFP, LAMP and LAMFP in Fig.1 are agreed with the orthorhombic structure LiMnPO₄ with a *Pnmb* space (PDF#74-0375) [50]. The carbon content of LMP, LMFP, LAMP and LAMFP is 6.6, 6.7, 6.5 and 6.7 wt.%, indicating that Fe and/or Al doping have little effect on the pyrolysis of sucrose. The peaks for carbon cannot be observed in Fig. 1 due to its amorphous structure [50].

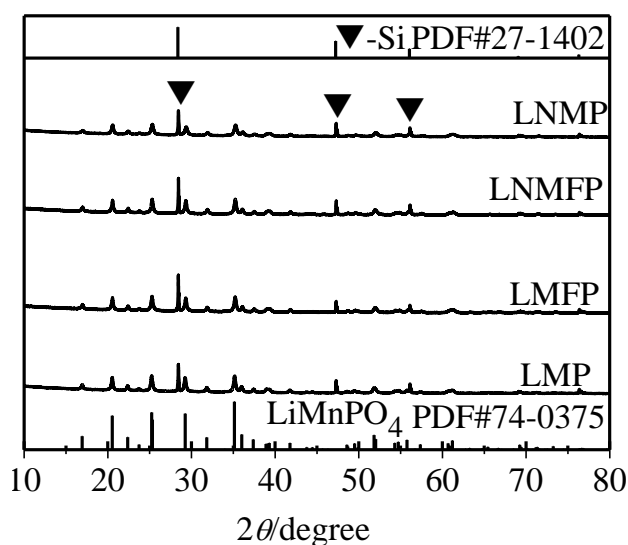
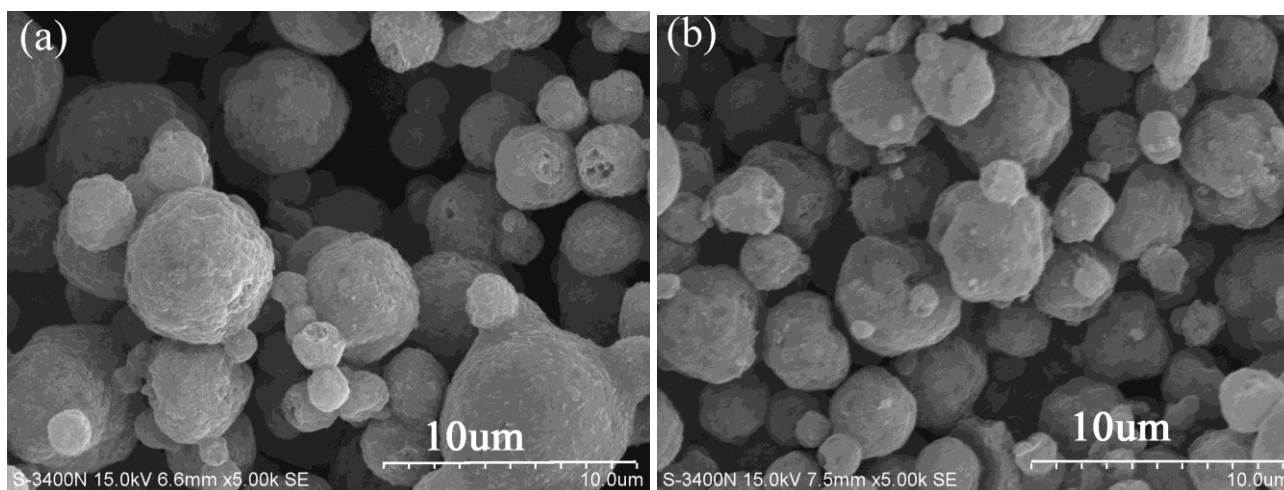


Figure 1. XRD patterns for the prepared samples. Powders were measured in the range from 10° to 80°. LiMnPO₄/C (LMP), LiMn_{0.85}Fe_{0.15}PO₄/C (LMFP), Li_{0.995}Al_{0.005}MnPO₄/C (LAMP) and Li_{0.995}Al_{0.005}Mn_{0.85}Fe_{0.15}PO₄/C (LAMFP)

Table 1. Cell parameters of pure and doped LiMnPO₄/C.

Sample	a/Å	b/Å	c/Å	V/Å ³
LMP	6.10198	10.44597	4.74422	302.4018
LMFP	6.08710	10.42723	4.73723	300.6795
LAMP	6.10201	10.44506	4.74322	302.3132
LAMFP	6.08697	10.42669	4.73926	300.7863

Table 1 presents the Cell parameters of the prepared samples. Obviously, Fe-doping results in a shrinkage in the lattice and a decreases in the unit cell volume and lengths (*a*, *b* and *c*) [24, 26, 38, 41, 44-48, 50], because the ionic radii of Mn²⁺ (0.83 Å) in octahedral coordination is larger than that of Fe²⁺ (0.78 Å) [58]. These results demonstrate that Fe is introduced into the Mn site of the olivine lattice to form a solid-solution in LiMnPO₄ matrix [24, 26, 38, 41, 44-48, 50]. Al doped on the Li site would lead to a shrinkage of crystal lattice, because the ionic radii of Al³⁺ (0.675 Å) is smaller than that of Li⁺ (0.76 Å) [58]. As given in Table 1, the lengths (*a*, *b* and *c*) and the cell volume of LAMP are smaller than that of LMP, indicating that Al is introduced into the Li site to form a solid-solution [51, 53-55]. As pointed by the previous reports [10, 41, 50, 56, 57], the nucleation of the second phase can be accelerated by the solid-solutions formed by doping Fe or Al in LiMnPO₄. Jahn-Teller effect induced lattice distortion has a great influence on the Li⁺ transport in LiMnPO₄ [10, 23, 50]. Hence, the Li⁺ transport can be improved by Fe or Al doping, since the shrinkage of unit cell of Fe or Al doped LiMnPO₄ can reduce the local distortion during the charge/discharge processes [23, 50]. The dynamic stability of LiMnPO₄ is worse than that of LiFePO₄ during cycling due to a large volume change (~9%) during the phase transition between LiMnPO₄ and MnPO₄ [12, 56, 57]. Fe or Al doped LiMnPO₄ should have a smaller volume changes because of its smaller unit cell volume, suggesting that Fe or Al doping can improve the dynamic stability of LiMnPO₄ [12, 50]. The ionic conductivity of LiMPO₄ (M = Mn, Fe or Co) can be enhanced by decreasing the *b* values, because the *b*-direction in the MnO₆ planes of the olivine structure is the only direction for the polaron-conduction [12, 50, 61-63].



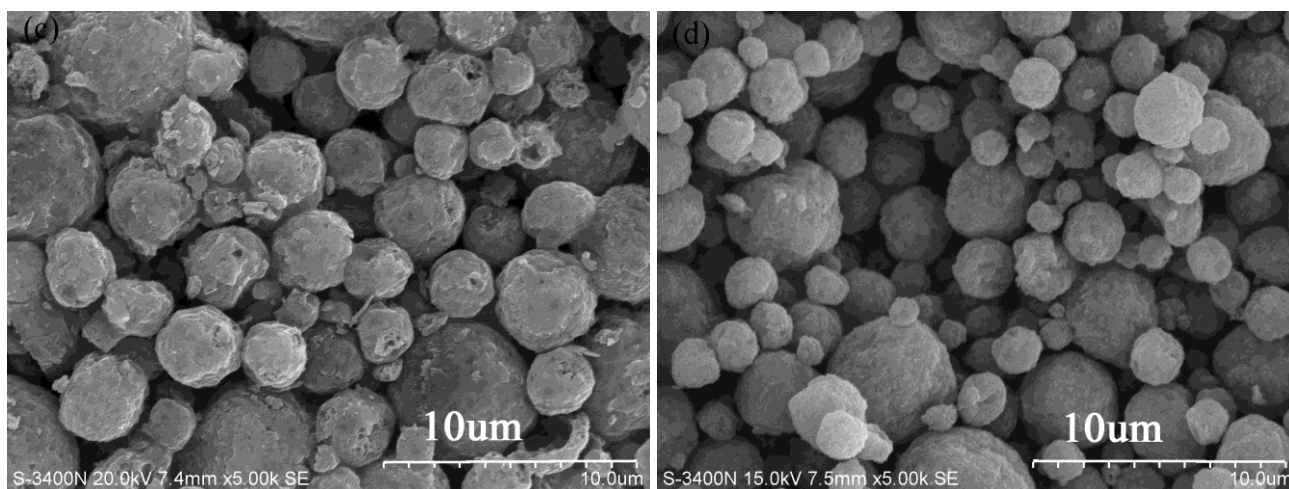
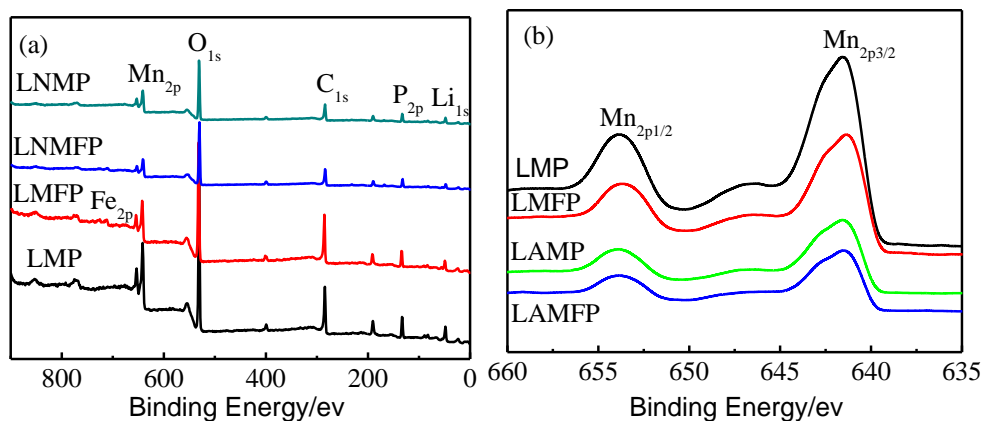


Figure 2. FESEM images of the prepared samples: (a) LiMnPO_4/C (LMP), (b) $\text{LiMn}_{0.85}\text{Fe}_{0.15}\text{PO}_4/\text{C}$ (LMFP), (c) $\text{Li}_{0.995}\text{Al}_{0.005}\text{MnPO}_4/\text{C}$ (LAMP) and (d) $\text{Li}_{0.995}\text{Al}_{0.005}\text{Mn}_{0.85}\text{Fe}_{0.15}\text{PO}_4/\text{C}$ (LAMFP).

Therefore, the ionic conductivity of LiMnPO_4 can be improved by Fe or Al doping, since the b values of LMFP and LAMP are smaller than that of LiMnPO_4 . As seen from Table 1, a , b , c and V of Fe-Al co-doped sample are smaller than that of Fe or Al doped sample, demonstrating that Fe-Al co-doping has a synergistic effect in the shrinkage of crystal lattice [24, 38, 41, 45-48, 50]. Therefore, the performance of LiMnPO_4 should be further improved by Fe-Al co-substitution. FESEM images presented in Fig.2 show that both of doped LiMnPO_4/C and undoped LiMnPO_4/C have pseudo-spherical morphology and similar particle sizes, indicating that Fe- and/or Al doping has little influence on the particle growth and the micromorphology [50].

The oxidation states of Fe, Al and Mn of the prepared samples were identified using XPS experiments [50]. Fig. 3 gives the XPS full spectra and high-resolution spectra of M (M= Mn, Fe) for LMP, LMFP, LAMP and LAMFP. Fe- and/or Al-doped samples have similar XPS spectra, and the peaks related to Li_{1s} , P_{2p} , C_{1s} , O_{1s} , Mn_{2p} and Fe_{2p} are labeled in Fig. 3(a) [50]. However, the reflections of Al are not visible in Fig. 3(a) due to its low content so that it cannot be detected by XPS. The peaks in Fig. 3(b) located at about 641 and 653 eV are related to $\text{Mn}_{2p_{3/2}}$ and $\text{Mn}_{2p_{1/2}}$, respectively, which are the characteristic for Mn^{2+} [24].



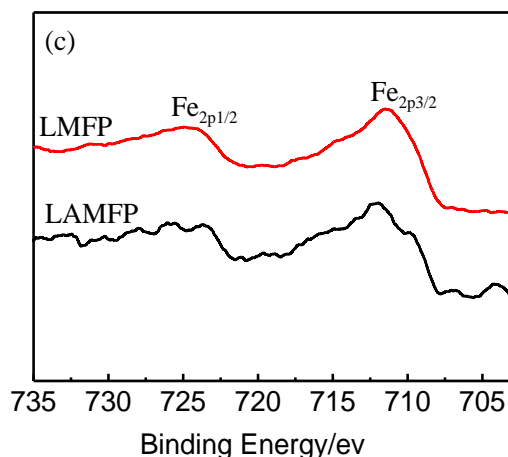


Figure 3. X-ray photoelectron spectroscopy of the prepared samples: (a) full spectra, (b) Mn_{2p} , and (c) Fe_{2p} . $LiMnPO_4/C$ (LMP), $LiMn_{0.85}Fe_{0.15}PO_4/C$ (LMFP), $Li_{0.995}Al_{0.005}MnPO_4/C$ (LAMP) and $Li_{0.995}Al_{0.005}Mn_{0.85}Fe_{0.15}PO_4/C$ (LAMFP)

The difference of Mn_{2p} spectra of LMP, LMFP, LAMP and LAMFP may be ascribed to the lattice deformation cause by the introduce Fe into Mn site and/or Al into Li site. The XPS peaks at ~ 711 and ~ 724 eV in Fig. 3(c) are ascribed to $Fe_{2p_{1/2}}$ and $Fe_{2p_{3/2}}$ [50, 54]. Therefore, the oxidation states of Mn and Fe in the prepared samples are +2, respectively [50]. The oxidation states of Al can be taken as +3 [55].

XPS results demonstrate that the oxidation state of Mn^{2+} in the Fe- and/or Al-doped samples is the same as that in $LiMnPO_4$ change. However, Fe^{2+} in LMFP can be oxidized to Fe^{3+} and form Fe^{3+} -vacancy pairs during the Li^+ extraction processes [56, 57]. In Al-doped samples, Al^{3+} introduced at the Li site can form Al^{3+} -vacancy pairs [50, 51, 55, 64, 65]. The electrode kinetics of $LiMnPO_4$ can be enhanced by, because the Mn^{2+}/Mn^{3+} redox reaction near localized Fe^{3+} -vacancy pairs and Al^{3+} -vacancy pairs can occur more easily than that surrounded by only Mn^{2+} - Li^+ pairs [10, 41, 50, 56-57]. Therefore, the electrochemical kinetics of $LiMnPO_4$ can be further improved by Fe^{2+} and Al^{3+} co-doping due to its synergistic effect on the formation of metal ion- vacancy pairs [50].

3.2. Electrochemical performance

Fig. 4 gives charge-discharge behaviors of pure and doped $LiMnPO_4/C$ at $25^\circ C$. As seen in Fig. 4(a), the charge/discharge plateaus situated at about 3.5 and 4.0 V vs. Li/Li^+ in the initial charge/discharge curves are related to the M^{2+}/M^{3+} ($M = Fe$ or Mn) redox couples, respectively [11,38,40,4, 50]. Moreover, the discharge plateau of Mn^{2+}/Mn^{3+} of Fe^{2+} - Al^{3+} co-doped sample increases to 4.0 V vs. Li/Li^+ [50]. Clearly, Fe^{2+} - Al^{3+} co-doping can significantly improve the discharge capacity of $LiMnPO_4$. As shown in Fig. 4(b), the discharge capacity of all samples decreases with the increase of the C rates [50]. LAMFP delivers capacities of 160, 147, 138, 113 and 62 $mAh \cdot g^{-1}$ at 0.2, 0.5, 1, 2 and 5 C, respectively. However, LMP only exhibits discharge capacities of 138, 107, 84, 61 and 20 $mAh \cdot g^{-1}$ at 0.2, 0.5, 1, 2 and 5 C, respectively. Therefore, the rate capability of $LiMnPO_4$ can significantly enhanced by Fe^{2+} and Al^{3+} co-doping.

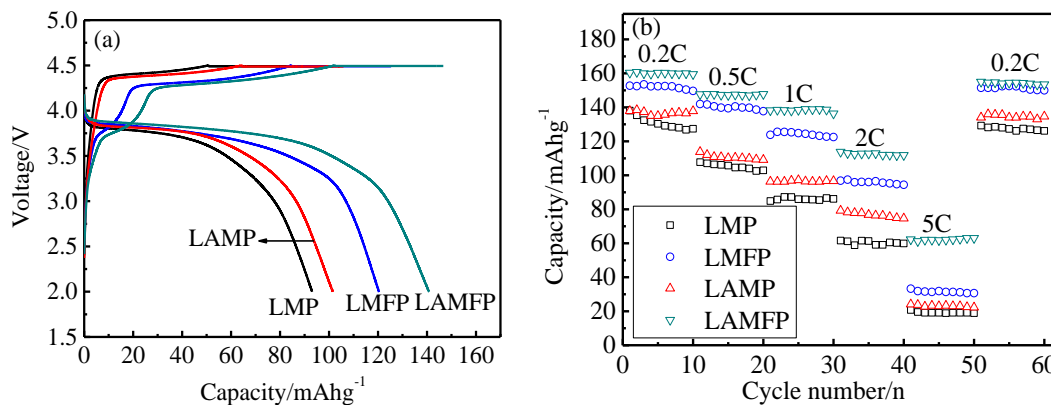


Figure 4. Electrochemical performance of the prepared samples at 25 °C: (a) Initial charge/discharge curves at 1 C (175 mA·g⁻¹) by CC-CV mode, and (b) rate performance at different C rates by CC-CV mode. LiMnPO₄/C (LMP), LiMn_{0.85}Fe_{0.15}PO₄/C (LMFP), Li_{0.995}Al_{0.005}MnPO₄/C (LAMP) and Li_{0.995}Al_{0.005}Mn_{0.85}Fe_{0.15}PO₄/C (LAMFP)

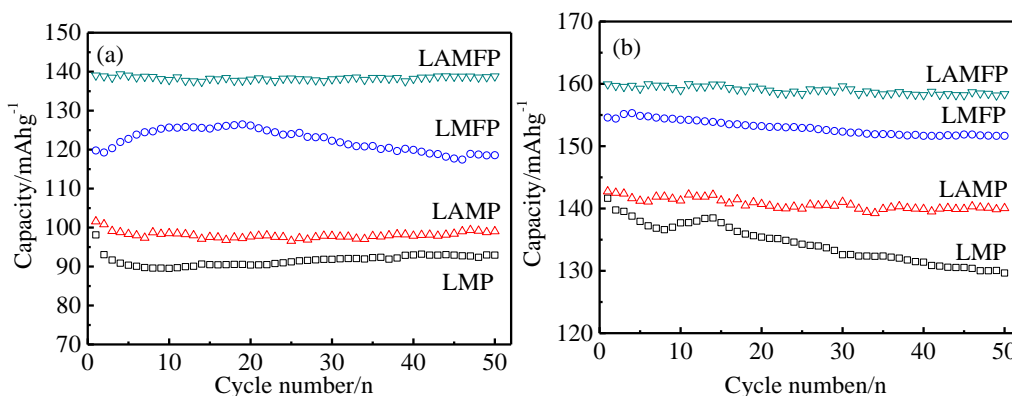


Figure 5. Cycling performance of the prepared samples at 1 C (175 mA·g⁻¹) by CC-CV mode: (a) 25 °C, (b) 60 °C. LiMnPO₄/C (LMP), LiMn_{0.85}Fe_{0.15}PO₄/C (LMFP), Li_{0.995}Al_{0.005}MnPO₄/C (LAMP) and Li_{0.995}Al_{0.005}Mn_{0.85}Fe_{0.15}PO₄/C (LAMFP)

Fig.5 gives the cycle behavior of pure and doped LiMnPO₄/C at 1 C rate. When charged and discharged at 25 °C, LMP, LMFP, LAMP and LAMFP give a discharge capacity of 98, 120, 101 and 139 mAh·g⁻¹, and the corresponding capacity retention is 95, 99, 98 and 100% after 50 cycles, respectively. When charged and discharged at 60 °C, LMP, LMFP, LAMP and LAMFP exhibit a discharge capacity of 135, 153, 143 and 160 mAh·g⁻¹, and the corresponding capacity retention is 96, 99.1, 98 and 99 % after 50 cycles, respectively. Therefore, the discharge capacity and the cycling stability of LiMnPO₄/C can be markedly improved by Fe²⁺ and Al³⁺ co-doping because of the synergistic effect between Fe²⁺ doping at the Mn-site and Al³⁺ doping at the Li-site [50], which are consistent with the results from Fig.1 and Fig.3, and can also be further confirmed by the EIS and CV experiments as given in Figs.6 and 7.

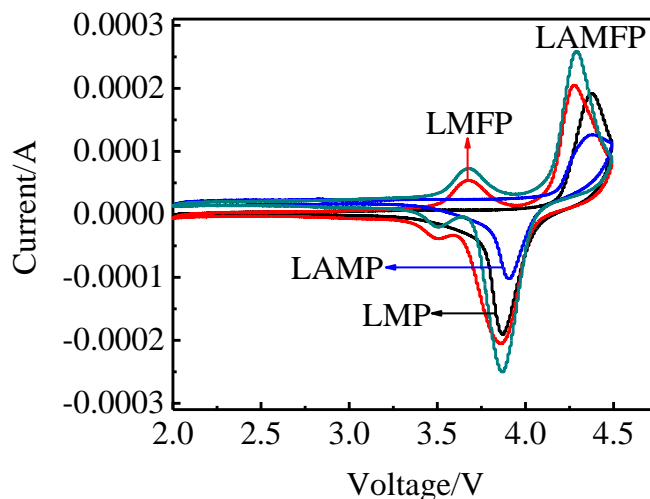


Figure 6. Cyclic voltammetry curves of the prepared samples after 2 cycles at 1 C by CC–CV mode. three electrode cells were measured between 2.0 and 4.5 V (vs. Li/Li⁺) at 0.2 mV s⁻¹ and 25 °C. LiMnPO₄/C (LMP), LiMn_{0.85}Fe_{0.15}PO₄/C (LMFP), Li_{0.995}Al_{0.005}MnPO₄/C (LAMP) and Li_{0.995}Al_{0.005}Mn_{0.85}Fe_{0.15}PO₄/C (LAMFP)

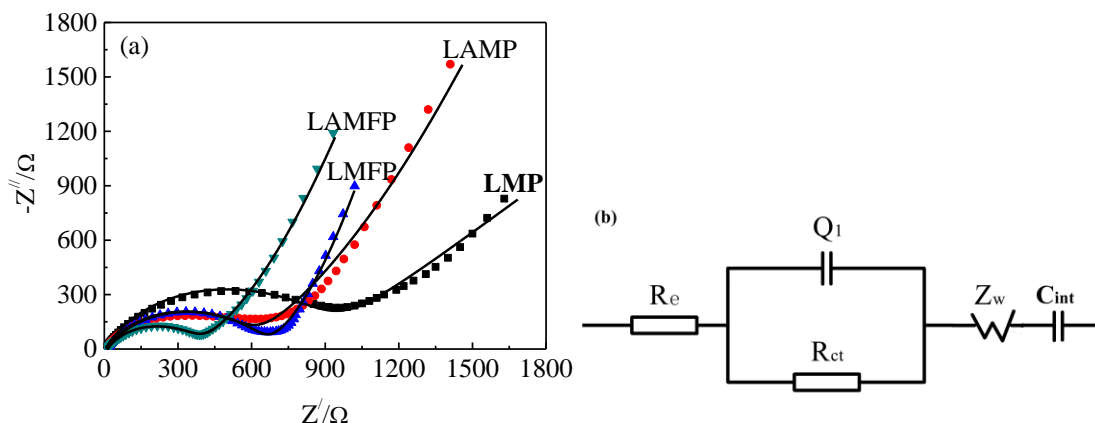


Figure 7. (a) Electrochemical impedance spectra after 2 cycles at 1 C by CC–CV mode and (b) equivalent circuit of the prepared samples. Three electrode cell were measured in the range of 100k Hz to 0.01 Hz at 25 °C. LiMnPO₄/C (LMP), LiMn_{0.85}Fe_{0.15}PO₄/C (LMFP), Li_{0.995}Al_{0.005}MnPO₄/C (LAMP) and Li_{0.995}Al_{0.005}Mn_{0.85}Fe_{0.15}PO₄/C (LAMFP)

The effects of Fe²⁺ and/or Al³⁺ doping on the electrode reaction were further investigated by CV and EIS experiments. Fig. 6 gives the CV curves of Fe²⁺ and/or Al³⁺ doped samples between 2.0 and 4.5 V (vs. Li/Li⁺) with a sweep rate of 0.2 mV s⁻¹ at 25 °C. As shown in Fig.6, the anodic and cathodic peaks centered at about 4.0 and 3.5 V can be ascribed to Mn²⁺/Mn³⁺ and Fe²⁺/Fe³⁺ redox couples, respectively [7, 9, 14, 40, 41, 50]. Furthermore, the shape of the anodic/cathodic peaks of LAMFP is more symmetrical and sharper than that of LMP, LMFP and LAMP, and the potential separations between the anodic and cathodic peaks at about 4.0 V are 0.52, 0.43, 0.48 and 0.42 V for LMP, LMFP, LAMP and LAMFP, respectively [50]. These data demonstrate that the reversibility of Li⁺ extraction/insertion in LiMnPO₄ can be highly enhanced by Fe²⁺-Al³⁺ co-doping [50].

Nyquist plots and the equivalent circuit of LMP, LMFP, LAMP and LAMFP are presented in Fig. 7. The EIS curves of the pure and doped samples include a compressed semicircle followed by an inclined line [9, 23, 24, 44, 50]. The ohmic resistance of the cell (R_e) can be represented by the high frequency intercept on the Z' -axis, while the compressed semicircle in the high and mid frequency region is mainly ascribed to the charge-transfer resistance (R_{ct}) and its capacities [38, 41, 45, 50]. The straight line in the low frequency expresses the Warburg impedance related to Li^+ diffusion in the LiMnPO_4/C particles [41, 45, 50]. The parameters of EIS obtained by the equivalent circuit in Fig. 7 (b) are given in Table 2. The electrode reactions are more favorable in the sample with a larger D_{Li^+} and a smaller R_{ct} [41, 45, 50]. Therefore, Fe^{2+} and Al^{3+} co-doped sample should have better rate performance because of its smallest R_{ct} and the largest D_{Li^+} , which is consistent with the charge/discharge measurements [50].

Table 2. Impedance parameters for the pure and doped LiMnPO_4/C

Sample	R_s / Ω		R_{ct} / Ω		$\sigma / \Omega \cdot \text{s}^{-0.5}$		D_{Li^+}
	Value	Error	Value	Error	Value	Error	$\text{cm}^2 \cdot \text{s}^{-1}$
LMP	5.3	3.3%	862.5	2.3%	386.6	6.3%	2.0×10^{-16}
LMFP	11.9	1.2%	636.2	0.7%	184.7	3.6%	8.8×10^{-16}
LAMP	6.4	5.3%	712.7	2.0%	206.4	4.3%	7.0×10^{-16}
LAMFP	4.1	7.6%	503.3	2.4%	198.3	6.3%	7.6×10^{-16}

In summary, $\text{Li}_{0.995}\text{Al}_{0.005}\text{Mn}_{0.85}\text{Fe}_{0.15}\text{PO}_4/\text{C}$ exhibits much better performance than that of $\text{LiMn}_{0.85}\text{Fe}_{0.15}\text{PO}_4/\text{C}$ and $\text{Li}_{0.995}\text{Al}_{0.005}\text{MnPO}_4/\text{C}$. The improvement of electrochemical performance can be ascribed to the synergistic effect of Fe^{2+} doping on the Mn site and Al^{3+} doping on the Li site [50].

4. CONCLUSIONS

A new solid-solution $\text{Li}_{0.995}\text{Al}_{0.005}\text{Mn}_{0.85}\text{Fe}_{0.15}\text{PO}_4/\text{C}$ has been prepared by a solid-state reaction. Fe^{2+} is introduced into the Mn site, and Al^{3+} is doped at the Li site of LiMnPO_4 . Fe^{2+} - Al^{3+} co-doping generates a synergistic effect in the shrinkage of unit cell and the creation of M^{3+} -vacancy pairs. $\text{Li}_{0.995}\text{Al}_{0.005}\text{Mn}_{0.85}\text{Fe}_{0.15}\text{PO}_4/\text{C}$ exhibits good rate performance and cycling stability. When charged and discharged with 1 C rate at 25 and 60 °C, this sample delivers a discharge capacity of 139 and 160 $\text{mAh} \cdot \text{g}^{-1}$, and its capacity retention ratio is about 100 % after 50 cycles. The enhanced property can be ascribed to the synergistic effect resulted from Fe^{2+} - Al^{3+} co-doping, because this synergistic effect can significantly enhance the structural stability, electrode kinetics and Li^+ diffusion rate. Thus, the electrochemical performance of LiMnPO_4 can be effectively improved by Fe^{2+} doping on the Mn site and aliovalent ion doping on the Li site.

ACKNOWLEDGEMENTS

The authors appreciate financial support from the National Natural Science Foundation of China (grant No. 21366006).

References

1. Z. Gong, Y. Yang, *Energy Environ. Sci.*, 4 (2011) 3223.
2. V. Aravindan, J. Gnanaraj, Y.S. Lee, S. Madhavi, *J. Mater. Chem. A*, 1 (2013) 3518.
3. J.O. Herrera, H. Camacho-Montes L.E. Fuentes, L. Álvarez- Contreras, *J. Mater. Sci. Chem. Eng.*, 3 (2015) 54.
4. L. Dimesso, C. Förster, W. Jaegermann, J. Khanderi, H. Tempel, A. Popp, J. Engstler, J. Schneider, A. Sarapulova, D. Mikhailova, *Chem. Soc. Rev.*, 41 (2012) 5068.
5. Z. Bakenov, I. Taniguchi, *Electrochem. Commun.*, 12 (2010) 75.
6. L. Wang, L.W. Zhang, J.J. Li, J. Gao, C.Y. Jiang, X.M. He, *Int. J. Electrochem. Sci.*, 7 (2012) 3362.
7. D. Di Lecce, J. Hassoun, *J. Phys. Chem. C*, 119 (2015) 20855.
8. S. Li, Z. Su, A. Muslim, X. Jiang, X. Wang, *Ceram. Int.*, 41 (2015) 11132.
9. L. Liao, H. Wang, H. Guo, P. Zhu, J. Xie, C. Jin, S. Zhang, G. Cao, T. Zhu, X. Zhao, *J. Mater. Chem. A*, 3 (2015) 19368.
10. N. Meethong, Y.H. Kao, M. Tang, H.Y. Huang, W.C. Carter, Y.M. Chiang, *Chem. Mater.*, 20 (2008) 6189.
11. S. Novikova, S. Yaroslavtsev, V. Rusakov, A. Chekannikov, T. Kulova, A. Skundin, *J. Power Sources*, 300 (2015) 444.
12. M. Köntje, M. Memm, P. Axmann, M. Wohlfahrt-Mehrens, *Prog. Solid State Chem.*, 42 (2014) 106.
13. J. Nava-Avendaño, M.R. Palacín, J. Oró-Solé, A. Ponrouch, J. M. Tarascon, N. Recham, *Solid State Ionics*, 263 (2014) 157.
14. K. Du, L.H. Zhang, Y.B. Cao, Z. D. Peng, G. R. Hu, *Mater. Chem. Phys.*, 136 (2012) 925.
15. G. Yang, H. Ni, H. Liu, P. Gao, H. Ji, S. Roy, J. Pinto, X. Jiang, *J. Power Sources*, 196 (2011) 4747.
16. S. Wi, J. Kim, S. Nam, J. Kang, S. Lee, H. Woo, M. Moosang Lee, C.H. Sonu, T. Moon, B. Park, *Curr. Appl Phys.*, 14 (2014) 725.
17. Q. Lu, G.S. Hutchings, Y. Zhou, H.L. Xin, H. Zheng, F. Jiao, *J. Mater. Chem. A*, 2 (2014) 6368.
18. Y. Dong, H. Xie, J. Song, M. Xu, Y. Zhao, J.B. Goodenough, *J. Electrochem. Soc.*, 159 (2012) A995.
19. G. Chen, A.K. Shukla, X. Song, T.J. Richardson, *J. Mater. Chem.*, 21 (2011) 10126.
20. M. Kotobuki, Y. Mizuno, H. Munakata, K. Kanamura, *Electrochemistry*, 79 (2011) 467.
21. Z. Bakenov, I. Taniguchi, *J. Electrochem. Soc.*, 157(2010) A430.
22. M.M. Doeff, J. Chen, T.E. Conry, R. Wang, J. Wilcox, A. Aumentado, *J. Mater. Res.*, 25 (2010) 1460.
23. J.W. Lee, M.S. Park, B. Anass, J.H. Park, M.S. Paik, S.G. Doo, *Electrochim. Acta*, 55 (2010) 4162.
24. T. Shiratsuchi, S. Okada, T. Doi, J.I. Yamaki, *Electrochim. Acta*, 54 (2009) 3145.
25. C. Nithya, R. Thirunakaran, A. Sivashanmugam, S. Gopukumar, *Chem. Asian J.*, 7 (2012)163-168
26. H. Yi, C. Hu, X. He, H. Xu, *Ionics*, 21 (2015) 667.
27. H. Fang, H. Yi, C. Hu, B. Yang, Y. Yao, W. Ma, Y. Dai, *Electrochim. Acta*, 71 (2012) 266.
28. Y. Zhang, Y. Zhao, L. Deng, *Ionics*, 18 (2012) 573.
29. J. Ni, L. Gao, *J. Power Sources*, 196 (2011) 6498.
30. L.Q. Kou, F.J. Chen, F. Tao, Y. Dong, L. Chen, *Electrochim. Acta*, 173 (2015) 721
31. Y. Gan, C. Chen, J. Liu, P. Bian, H. Hao, A. Yu, *J. Alloys Compd.*, 620 (2015) 350.

32. L. Wu, S. Zhong, J. Lu, J. Liu, F. Lv, *Ionics*, 19 (2013) 1061.
33. D.G. Kellerman, Y.G. Chukalkin, N.I. Medvedeva, M.V. Kuznetsov, N.A. Mukhina, A.S. Semenova, V.S. Gorshkov, *Mater. Chem. Phys.*, 149 (2015) 209.
34. E. Dai, H. Fang, B. Yang, W. Ma, Y. Dai, *Ceram. Int.*, 41 (2015) 8171.
35. L. Su, X. Li, H. Ming, J. Adkins, M. Liu, Q. Zhou, J. Zheng, *J. Solid State Electrochem.*, 18 (2014) 755.
36. A. Gutierrez, R. Qiao, L. Wang, W. Yang, F. Wang, A. Manthiram, *Chem. Mater.*, 26 (2014) 3018.
37. D. Kellerman, N. Medvedeva, N. Mukhina, A. Semenova, I. Baklanova, L. Perelyaeva, V. Gorshkov, *Chem. Phys. Lett.*, 591 (2014) 21.
38. J. Duan, G. Hu, Y. Cao, K. Du, Z. Peng, *Ionics*, 1 (2015)1.
39. S. Liu, H. Fang, E. Dai, B. Yang, Y. Yao, W. Ma, Y. Dai, *Electrochim. Acta*, 116 (2014) 97.
40. K. Kisu, E. Iwama, W. Onishi, S. Nakashima, W. Naoi, K. Naoi, *J. Mater. Chem. A*, 2 (2014) 20789.
41. V. Ramar, P. Balaya, *PCCP*, 15 (2013) 17240.
42. D. Jang, K. Palanisamy, J. Yoon, Y. Kim, W.S. Yoon, *J. Power Sources*, 244 (2013) 581.
43. H. Yi, C. Hu, H. Fang, B. Yang, Y. Yao, W. Ma, Y. Dai, *Int. J. Electrochem. Sci.*, 7 (2012) 663.
44. H. Fang, E. Dai, B. Yang, Y. Yao, W. Ma, *J. Power Sources*, 204 (2012) 193.
45. H. Yi, C. Hu, H. Fang, B. Yang, Y. Yao, W. Ma, Y. Dai, *Electrochim. Acta*, 56 (2011) 4052.
46. C. Hu, H. Yi, H. Fang, B. Yang, Y. Yao, W. Ma, Y. Dai, *Electrochem. Commun.*, 12 (2010) 1784.
47. J. Kim, Y.U. Park, D.H. Seo, J. Kim, S.W. Kim, K. Kang, *J. Electrochem. Soc.*, 158 (2011) A250.
48. W. Xiang, Y. Zhong, Y. Tang, H. Shen, E. Wang, H. Liu, B. Zhong, X. Guo, *J. Alloys Compd.*, 635 (2015) 180.
49. C. Sronsri, P. Noisong, C. Danvirutai, *Spectrochim. Acta, Part A*, 153 (2016) 436.
50. Q. Y. Huang, Z. Wu, J. Su, Y.F. Long, X.Y. Lv, Y.X. Wen, *Ceram. Int.*, 42 (2016) 11348
51. S.Y. Chung, J. T. Bloking, Y.M. Chiang, *Nat. Mater.*, 1 (2002) 123.
52. K. Hoang, M. D. Johannes, *J. Power Sources*, 206 (2012) 274.
53. J. Molenda, A. Kulka, A. Milewska, W. Zając and K. Świerczek, *Materials*, 6(2013) 1656
54. R. Kapaev, S. Novikova, T. Kulova, A. Skundin, A. Yaroslavtsev, *J. Solid State Electrochem.*, 19 (2015) 2793.
55. A. Kulka, A. Braun, T.-W. Huang, A. Wolska, M. T. Klepka, A. Szewczyk, D. Baster, W. Zając, K. Świerczek, J. Molenda, *Solid State Ionics*, 270 (2015) 33.
56. J. Kim, D. H. Seo, S.W. Kim, YU. Park, K. Kang, *Chem. Commun.*, 46 (2010) 1305.
57. D.H. Seo, H. Gwon, S.W. Kim, J. Kim, K. Kang, *Chem. Mater.*, 22 (2010) 518.
58. R.T. Shannon, *Acta Crystallogr., Sect. A*, 32 (1976) 751.
59. A.P. Grosvenor, B.A. Kobe, M.C. Biesinger, N.S. McIntyre, *Surf. Interface Anal.*, 36 (2004) 1564.
60. S. Zhang, Q. Wu, C. Deng, F. L. Liu, M. Zhang, F. L. Meng, H. Gao, *J. Power Sources*, 218(2012) 56.
61. R. Amin, P. Balaya, J. Maier, *Solid-State Lett.*, 10 (2007) A13.
62. P. Zhang, D. Zhang, L. Huang, M. Lin, Q. Wei, *J. Alloys Compd.*, 540 (2012) 121
63. P. Zhang, Y. Wu, D. Zhang, Q. Xu, J. Liu, X. Ren, Z. Luo, *J. Phys. Chem. A*, 112 (2008) 5406.
64. K. Hoang, M. Johannes, *Chem. Mater.*, 23 (2011) 3003.
65. M.S. Islam, D.J. Driscoll, C.A. Fisher, P.R. Slater, *Chem. Mater.*, 17 (2005) 5085.